Imperial College London

Department of AERONAUTICS

Theoretical, Computational, and Experimental Approaches to Indeterminate Beams: A Comparative Study

Lukas Campbell
02627000

Abstract

This report aims to investigate the bending behaviour of a statically indeterminate beam under three complementary approaches – analytical (Euler-Bernoulli beam theory), computational (1D vs. 3D finite element methods), and experimental measurements. A 0-40 N load sweep at Hanger 2 established near-perfect linearity ($R^2 \geq 0.999$) for experimental data, confirming negligible hysteresis and validating linear elasticity assumptions. The 1D beam-element model yielded deflection and strain slopes within 0.03% of theoretical expectations, the correlation being attributed to both methods using the same strain-moment relationships. By contrast, the 3D solid-element model (C3D8R) exhibited higher relative errors – approximately 8.079% in deflection and over −20.814% – due to inherent constraints in discretization that are introduced by the specific beam geometry. Convergence rates showed similar power-law trends for both methods, with 3D simulations however demanding substantially more computational time. Overall, the 1D approach proved optimal for this setup, offering fast convergence and high fidelity. Experimental errors remained small, arising mostly from boundary-condition variations and potential alignment issues. Findings underscore the possible trade-off between the broader applicability and efficiency & accuracy.

May 22, 2025

Contents

List of Figures

List of Tables

Nomenclature

Symbol	Definition	Unit
P_1	Load at support C	N
P_2	Load at Hanger 2	N
L	Length of beam	mm
h	Height of beam	mm
w	Width of beam	mm
E	Young's Modulus	Pa
I	Second Moment of Area	m^4
ν	Poisson's Ratio	–
${}^{i}V_X$	Vertical reaction at support $X \in \{A, B\}$ for determinate case $i \in \{1, 2\}$	
	$i = 1 \rightarrow$ load at C, $i = 2 \rightarrow$ load at Hanger 2	N
${}^{i}c$	Integration constant for deflection equations in determinate case i	
	$i = 1 \rightarrow$ load at C, $i = 2 \rightarrow$ load at Hanger 2	–

1 Introduction

Beam theory provides a framework for understanding the state responses of structural elements under transverse loading, playing fundamental roles in civil, mechanical, and aerospace engineering. The study of beams is the study of stresses, strains, and deflections, which enable accurate predictions of structural behaviour under various loading conditions. This report compares analytical, experimental, and computational methods for the analysis of beam deflections and strains, focusing on the accuracy and limitations of each approach.

Euler-Bernoulli beam theory, first formulated by Leonhard Euler and Daniel Bernoulli in the 18th century, remains widely used for predicting beam behaviour under small deflections. While it assumes plane sections remain plane, and neglects shear deformation, its simplicity is what makes it such a powerful tool for structural analysis. [1] Extensions of Euler-Bernoulli beam theory, such as Timoshenko beam theory, account for shear deformation and rotational inertia, improving the accuracy for short as well as deep beams. [2] Experimental validation remains crucial for an assessment of applicability in theoretical predictions.

Numerous factors often introduce discrepancies between theoretical and measured values, particularly material imperfections, boundary conditions, and load distribution. Computational methods – particularly Finite Element Analysis (FEA) – provide bridges between theory and experiment by numerically approximating beam behaviour under complex conditions which are analytically infeasible or unsolvable.

Experimental Setup

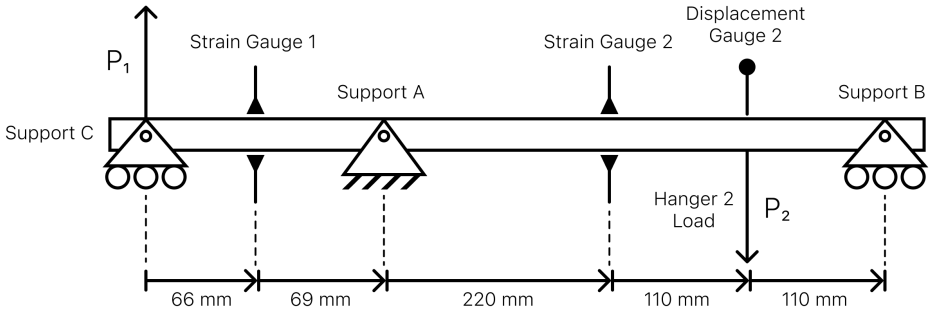

Figure 1: Model setup for computational, theoretical, and experimental trials

Figure 1 illustrates the idealized system modeled in the experimental, theoretical, and computational analyses. While the experimental setup includes strain and deflection gauges for measurement, the theoretical and computational models do not incorporate the gauges themselves but instead use their respective locations to evaluate strain and displacement.

During the experiment, zero-readings were taken and individual gauge precisions noted. This was followed by an incremental loading of $5\ \mathrm{N}$ to Hanger 2 (P_2) up until $40\ \mathrm{N}$ – followed by decrements of the same magnitude. This allowed for the evaluation of hysteresis, which was found to be negligible. Each gauge recording was taken within 10 seconds of the increment, in an attempt to minimize potential creep. Strain gauge voltage readings were converted to strain using a conversion factor of $0.943\ \mu\varepsilon/\mathrm{mV}$. [3] All analysis in this report uses a local reference frame treating positive *y* as "up".

2 FE Model Setup and Mesh Convergence Studies

The 3D setup consisted of an extruded beam profile matching that in Figure 1, with a total length of $L = 575$ mm and a rectangular cross-section measuring $w = 18.86$ mm in width and $h = 2.94$ mm in height. The material was assigned a Young's modulus of $E = 200$ GPa and a Poisson's ratio of $\nu = 0.3$. The boundary conditions were modeled to replicate the experimental setup, with support A fully constrained in translation, while supports B and C permitted only axial displacement, restricting both lateral and transverse translation. All supports allowed free rotation. A multi-point constraint (MPC) was applied at the soffit of the beam's cross-section at the axial location of Hanger 2, with this surface slaved to the reference node to ensure an even distribution of the applied load. The 1D setup was primarily identical to the 3D setup, with the only differences being that it was modeled as a 1D line, with the load applied as a concentrated point load. The reference system used treats positive as up for all calculations.

Python scripts where developed which interfaced with the Abaqus FEA API. The scripts ran the analysis for both cases, and extracted maximum strain and deflection values for each mesh size (including the gauge locations for the 1D case). Discretization used C3D8R in the 3D case, and 1D elements with a cubic formulation type for the 1D case. Mesh sizes ran from 100 mm to 0.0581 mm, and from 287.5 mm to 2 mm for the 1D and 3D cases respectively (due to node limits and numerical instability). Figure 2 illustrates the behaviour of deflections and strains with increasing mesh density at a 40 N applied load at Hanger 2. Mesh sizes of 2 mm and 0.0581 mm were chosen for all further analysis respectively, as convergence of neighbouring sizes far exceeded the precision of experimental data.

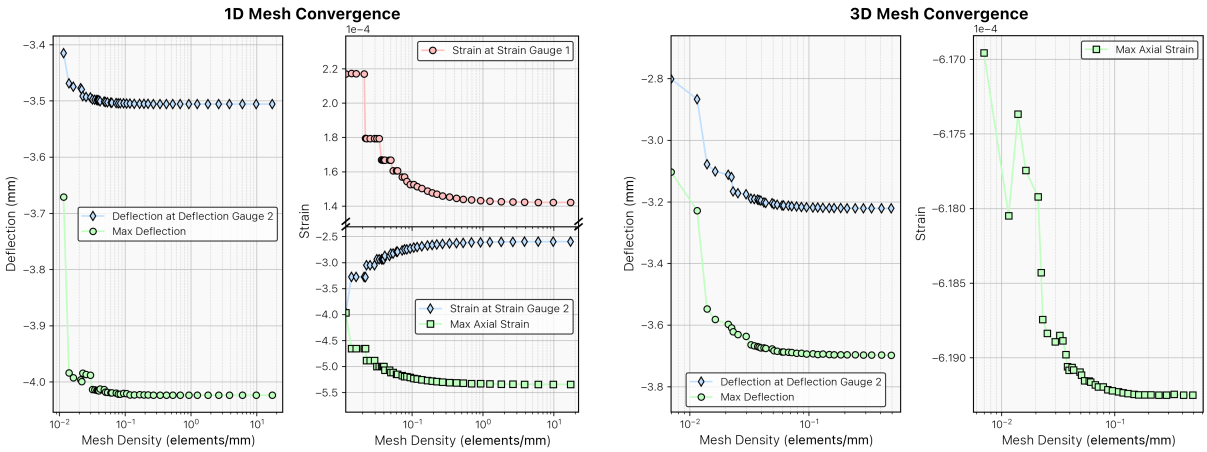

Figure 2: Convergence at different locations and mesh sizes, for 1D and 3D meshes

FEA Type	Measurement Location	Convergence Rate	R^2 Value	Asymptotic Value	*Relative Error (%)
1D	Max Deflection	11.5539	0.9608	-4.0236 mm	-0.02423
	Deflection Gauge 2	2.4331	0.9501	-3.5057 mm	-0.0306
	Max Strain	1.1175	0.9483	-534.6176 με	0.01215
	Strain Gauge 1	0.8953	0.9375	142.1042 με	0.07669
	Strain Gauge 2	1.1149	0.9465	-259.7285 με	-0.03403
3D (C3D8R)	Max Deflection	1.5345	0.9197	-3.6977 mm	8.0780
	Deflection Gauge 2	1.3384	0.9253	-3.2215 mm	8.0794
	Max Strain	0.9468	0.8749	-619.2503 με	-15.8164
	Strain convergence data not available for gauge locations				

*Relative to beam theory maxima

Table 1: Mesh Convergence Analysis using Power Law

3 Results and Discussions

To begin, we first set up equilibrium equations for the two determinate cases. This yields

$$\begin{matrix}\Sigma F_y \\ \Sigma M_A\end{matrix}\begin{vmatrix} \\ \end{vmatrix} \quad \begin{bmatrix}1 & 1\\ 0 & 0.440\end{bmatrix}\begin{bmatrix}{}^1V_A\\ {}^1V_B\end{bmatrix} = P_1\begin{bmatrix}-1\\ 0.135\end{bmatrix} \quad \begin{bmatrix}1 & 1\\ 0 & 0.440\end{bmatrix}\begin{bmatrix}{}^2V_A\\ {}^2V_B\end{bmatrix} = P_2\begin{bmatrix}1\\ 0.330\end{bmatrix} \tag{1}$$

where the matrix equations correspond to the respective determinate loading case[1]. After inverting and solving, setting up our moment and deflection equations is trivial. Using the double integration method yields

$$-EIv(x) = \iint_0^x M(x)\mathrm{d}x \tag{2}$$

$$M_1(x) = P_1\big(\langle x\rangle - 1.307\langle x-0.135\rangle\big) \tag{3}$$

$$M_2(x) = P_2\big(0.25\langle x-0.135\rangle - \langle x-0.465\rangle\big) \tag{4}$$

$$\Rightarrow v_1(x) = \frac{P_1}{6EI}\big(\langle x\rangle^3 - 1.307\langle x-0.135\rangle^3 + {}^1c_1x + {}^1c_2\big) \tag{5}$$

$$\Rightarrow v_2(x) = \frac{P_2}{6EI}\big(0.25\langle x-0.135\rangle^3 - \langle x-0.465\rangle^3 + {}^2c_1x + {}^2c_2\big) \tag{6}$$

Next, the system boundary conditions $v_i(j) = 0,\ \forall i \in \{1,2\},\ j \in \{0.135, 0.575\}$ are applied, which yields the following matrices

$$\begin{bmatrix}0.135 & 1\\ 0.575 & 1\end{bmatrix}\begin{bmatrix}{}^1c_1\\ {}^1c_2\end{bmatrix} = -\begin{bmatrix}0.00246\\ 0.0788\end{bmatrix} \quad \begin{bmatrix}0.135 & 1\\ 0.575 & 1\end{bmatrix}\begin{bmatrix}{}^2c_1\\ {}^2c_2\end{bmatrix} = \begin{bmatrix}0\\ -0.0200\end{bmatrix} \tag{7}$$

Once inverted and solved, the superposition boundary condition $v_1(0) + v_2(0) = 0$ can be applied, which finally yields the following relationship (as all terms but c_2 drop out at 0)

$$v_1(0) + v_2(0) = 0 \Rightarrow 0.000437P_1 + 0.000128P_2 = 0 \Rightarrow P_1 = -0.292P_2 \tag{8}$$

Now that a relationship between the reaction force at support C and the applied load at Hanger 2 has been established, this process can be repeated for a single case with both forces present, ultimately generating the strain and deflection equations for the indeterminate case. After numerical substitution, this yields the following equations[2]

$$M(x) = P_2\big(0.292\langle x\rangle - 0.632\langle x-0.135\rangle - \langle x-0.465\rangle\big) \tag{9}$$

$$\varepsilon(x) = \frac{M(x)y}{EI} = 3.07\times10^{-5}M(x) \tag{10}$$

$$v(x) = \frac{P_2}{47.927}\big(0.292\langle x\rangle^3 - 0.632\langle x-0.135\rangle^3 - \langle x-0.465\rangle^3 - 1.11\times10^{-4}x\big) \tag{11}$$

[1] Refer to Figure 1 for a reminder on setup

[2] Note: All equations in base SI units

Once theoretical moment and elastic relationships were established, load sweeps for both computational methods were performed across the discrete experimental load domain.

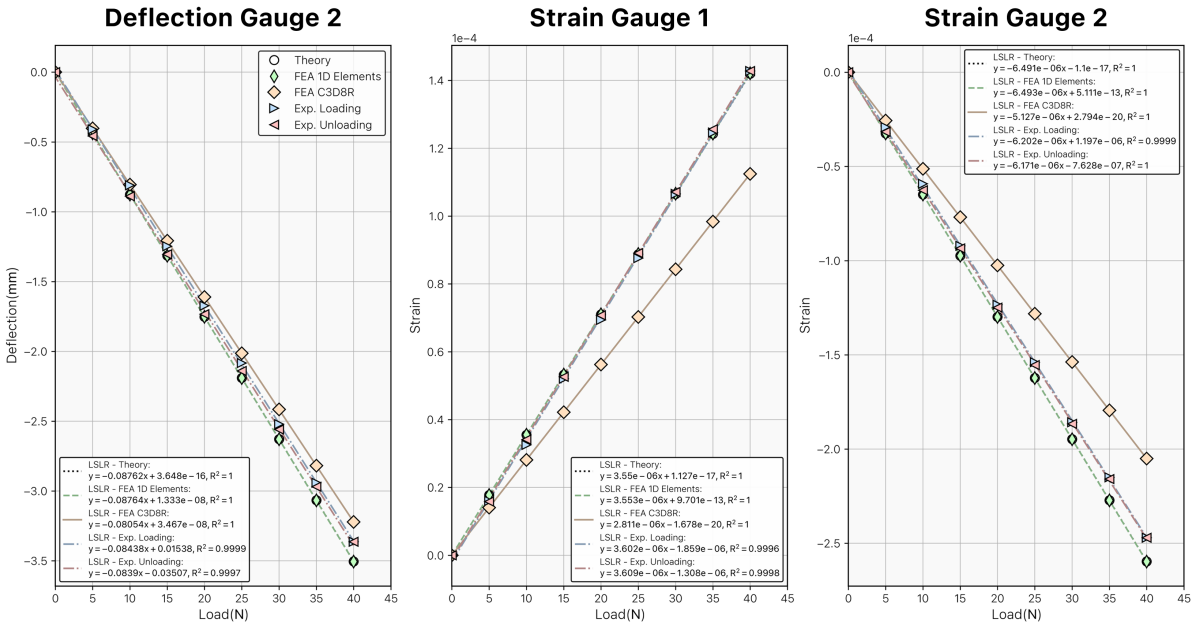

Figure 3: Load vs. Displacement Curves for All Methods

Analysis Method	Displacement			Strain Gauge 1			Strain Gauge 2		
	Gradient (mmN^{-1})	Error (%)	R^2 Value (−)	Gradient ($\mu\varepsilon N^{-1}$)	Error (%)	R^2 Value (−)	Gradient ($\mu\varepsilon N^{-1}$)	Error (%)	R^2 Value (−)
Elastic Curve	-0.0876	N/A	1.000	3.550	N/A	1.000	-6.491	N/A	1.000
Experimental – Loading	-0.0844	3.692	0.9999	3.602	1.467	0.9996	-6.202	4.446	0.9999
Experimental – Unloading	-0.0840	4.246	0.9997	3.602	1.662	0.9998	-6.202	4.9210	1.000
FEA (1D)	-0.0876	-0.0310	1.000	3.553	0.077	1.000	-6.493	-0.034	1.000
FEA (C3D8R)	-0.0805	8.079	1.000	2.811	-20.814	1.000	-5.127	21.014	1.000

*Relative to beam theory

Table 2: Load Dependent Gradient Errors

Figure 3 describes the data produced by each method. Least squares regression lines (LSLR) were used to calculate the load dependent gradients, the results of which are summarized in Table 2. Ultimately, extremely linear relationships were observed in all methods (with R^2 values of 1 for both theoretical and computational methods). The linearity observed in experimental results confirms that the assumption of linear elasticity holds, and that both the computational and theoretical models used should accurately predict behaviour.

Furthermore, no hysteresis is present as the loading and unloading curves differ negligibly for the experimental fit. It should be clear from Table 2 that the 1D FEA far surpasses the experimental, and the other computational method, consistently having errors several orders of magnitude lower. This naturally follows from its direct application of (9) and (10), which makes it particularly effective at modeling the axial strains. Conversely, the 3D FEA encountered challenges in effectively capturing the behaviour of the beam. This can likely be attributed to the way mesh discretization occured. Vertical mesh resolution was quite low, being inherently constrained by the beams geometry. Each new vertical layer of elements necessitates a

significantly larger number of transverse elements, which increases computational demand to infeasible levels. These new transverse elements provide no significant increase in accuracy when attempting to describe strain distribution. This explains the higher relative accuracy in deflection observations, when compared to strain, as the strain distribution could not be accurately captured before a computational ceiling was reached. This is not something the 1D FEA suffered from, as its discretization only relied on one-dimensional points. Additionally, the relationship between moment and strain in (10) signifies that vertical discretization elements are not required – the relationship is simply linear – and thus mesh resolution can be much higher.

To supplement the previous discussion on computational accuracy, Table 1 quantifies convergence characteristics and results for the two computational methods. The 1D FEA achieves a faster general convergence than the 3D FEA, however it should be noted that the particular convergence rates (bar maximum deflection for the 1D FEA), are quite similar in both cases. The computational time required for each method however differed drastically, with the 3D FEA taking significantly longer to compute a single mesh size. Additionally, the relative error in the asymptotic values is significantly lower for the 1D FEA than for the 3D FEA, which naturally follows from the numerical relationship between moment and strain described earlier. Both results exhibit a power-law trend, suggesting asymptotic behavior as the mesh is refined further. The accuracy of this behaviour is further supported by the high R^2 values, suggesting a high level of confidence. Ultimately, using 3D FEA has no benefits in this setup, as it is less accurate, and more computationally expensive, while having no real convergence rate benefit.

The experimental method proved more accurate than the 3D FEA, and ultimately discrepancies between the experimental method and beam theory are simply derived from errors accumulated during the procedure. Instrumentation precision has negligible effect, as the deflection gauge had a precision of $0.001\,\text{mm}$ and the strain gauges a precision of $0.943 \times 10^{-8}\varepsilon$, which are practically negligible in the context of this comparison. Discrepancies thus arise from practical factors – slight variations in support locations, and potential misalignments – and from the idealized assumptions made about the system.

4 Conclusion

Consistent with assumptions of linear elasticity, both computational models and the theoretical elastic curve produced functionally perfect linear correlations (R^2 values of 1) for every load sweep and the corresponding strain and deflection data. The 1D and 3D beam models both converged with relatively close rates (bar maximum deflection for the 1D). The 1D beam model accurately matched beam theory, with minimal computational cost. In contrast, the 3D FEA required significantly finer meshes to capture the thin cross-section's strain gradients (and wasn't able to fully before reaching the softwares computational ceiling), thereby increasing the computational demand. Nonetheless, all computational approaches were able to accurate characterize the global deflection behaviour. Experimentally, strain and deflection gauge readings were able to validate the linearity of the system, with negligible hysteresis observed, even over multiple loading/unloading cycles. Instrument precision was low enough as to be considered functionally negligible. Discrepancies between the theoretical prediction and the experimental results are thus due to slight variations in support locations and potential misalignments, in addition to the broad simplifications made in our idealized system. Overall, this study confirms that the simpler 1D beam-element approach remains a highly efficient and accurate tool for the analysis of slender beams under bending, and while the 3D approach was not as accurate, it is a more versatile approach for capturing more complex systems.

References

[1] Wikipedia contributors. Euler–Bernoulli beam theory — Wikipedia, The Free Encyclopedia; 2025. Accessed: 2025-03-03. Available from: https://en.wikipedia.org/wiki/Euler%E2%80%93Bernoulli_beam_theory.

[2] Wikipedia contributors. Timoshenko–Ehrenfest beam theory; 2023. [Online; accessed 04/03/2025]. Available from: https://en.wikipedia.org/wiki/Timoshenko%E2%80%93Ehrenfest_beam_theory.

[3] Robinson P. Behaviour of Simple Beams - First Year Laboratory. 2017.

Appendix A: Power Law Fits

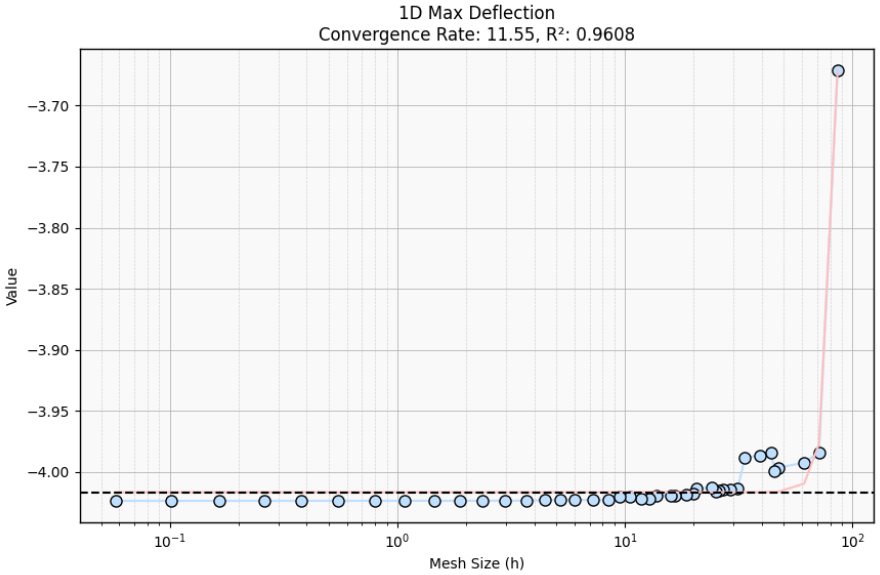

Figure 4: 1D Max Deflection Convergence

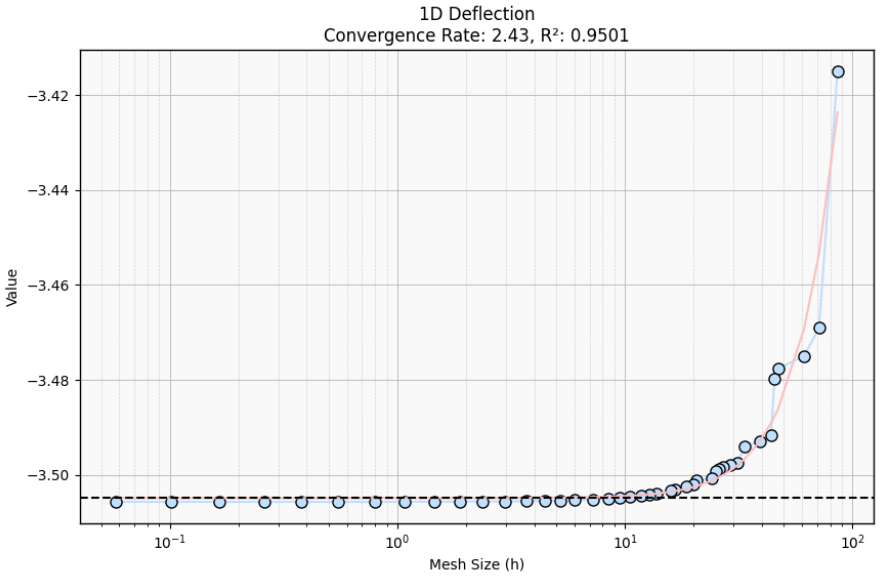

Figure 5: 1D Deflection Convergence

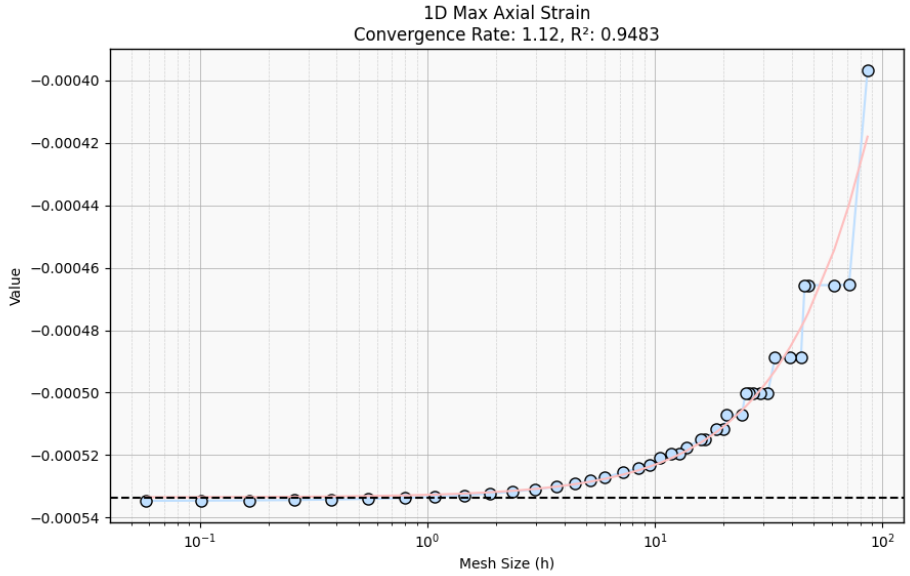

Figure 6: 1D Max Strain Convergence

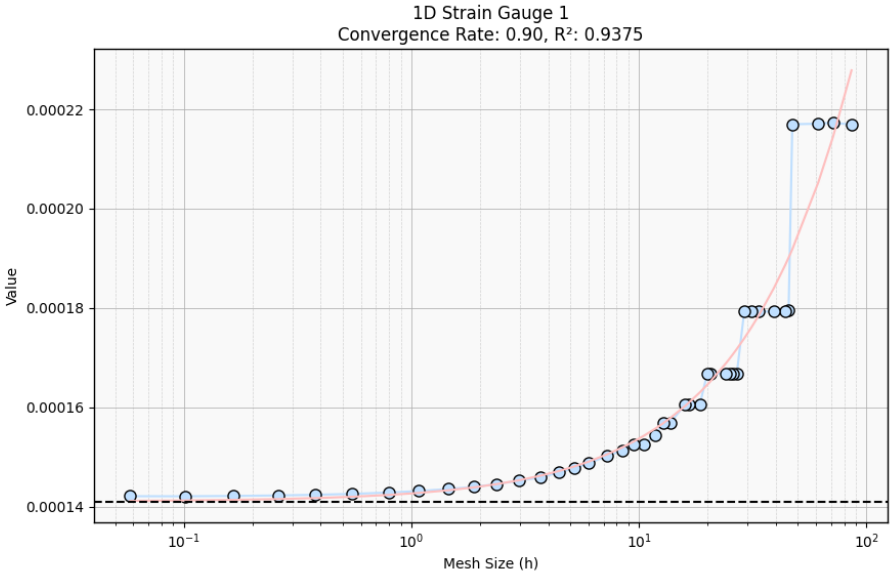

Figure 7: 1D Strain Gauge 1 Convergence

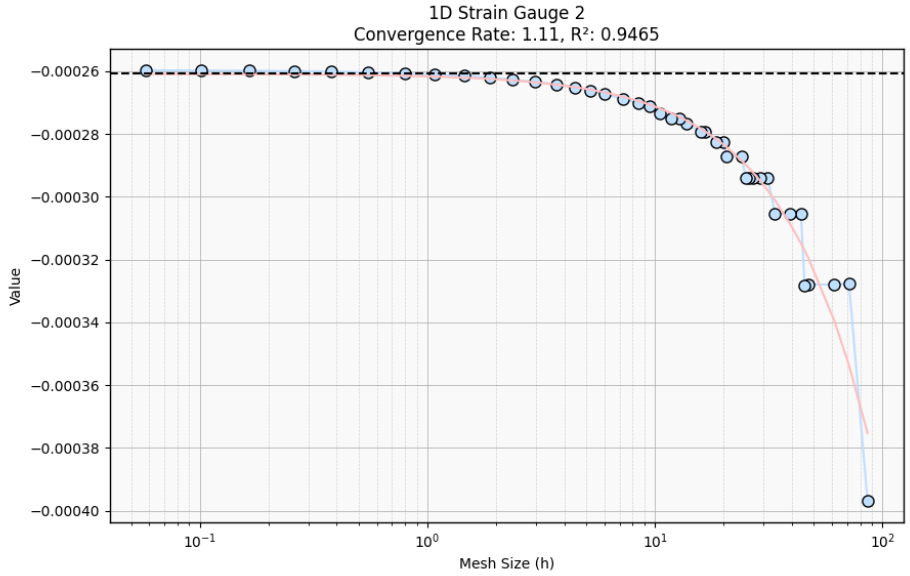

Figure 8: 1D Strain Gauge 2 Convergence

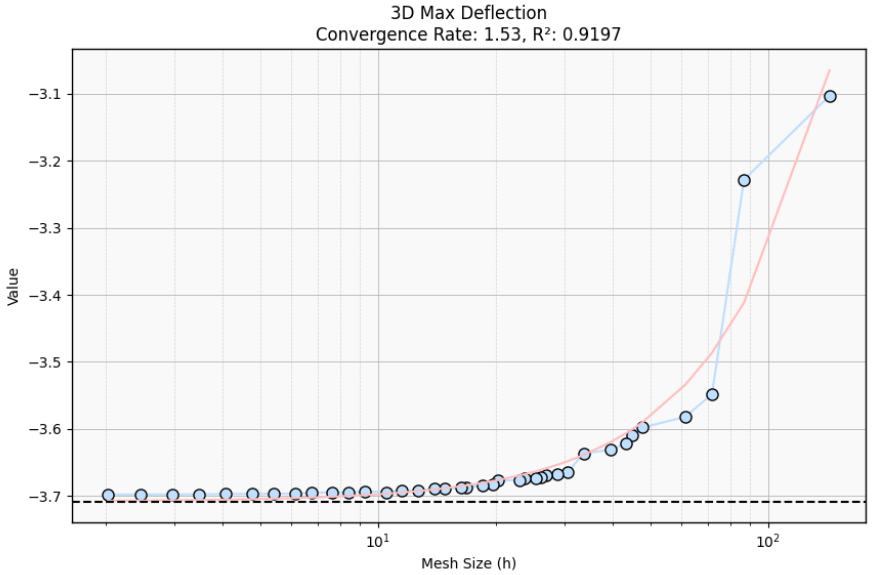

Figure 9: 3D Max Deflection Convergence

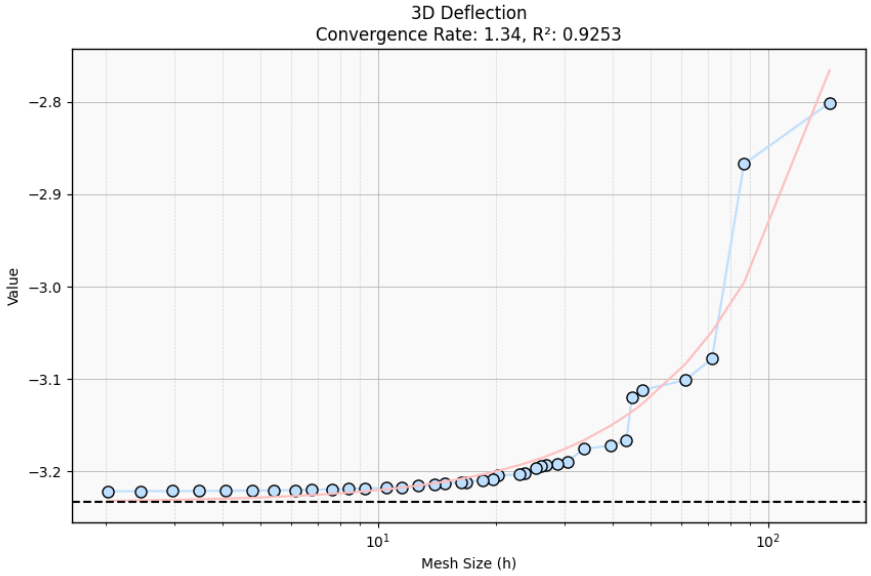

Figure 10: 3D Deflection Convergence

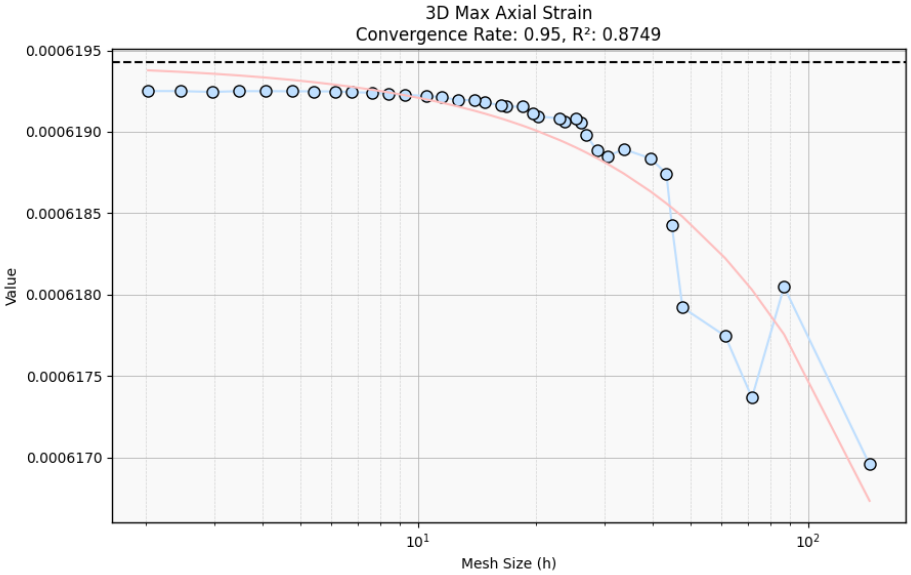

Figure 11: 3D Max Strain Convergence